View metadata, citation and similar papers at core.ac.uk
brought to you by CORE
provided by DSpace@MIT

Invited Paper

Optical Stark effect in 2D semiconductors

Edbert J. Sie[a], James W. McIver[b], Yi-Hsien Lee[c], Liang Fu[a], Jing Kong[a], and Nuh Gedik*[a]
[a]Massachusetts Institute of Technology, Cambridge, MA 02139, USA; [b]Max Planck Institute for the Structure and Dynamics of Matter, Hamburg 22761, Germany; [c]National Tsing-Hua University, Hsinchu 30013, Taiwan

ABSTRACT

Semiconductors that are atomically thin can exhibit novel optical properties beyond those encountered in the bulk compounds. Monolayer transition-metal dichalcogenides (TMDs) are leading examples of such semiconductors that possess remarkable optical properties. They obey unique selection rules where light with different circular polarization can be used for selective photoexcitation at two different valleys in the momentum space. These valleys constitute bandgaps that are normally locked in the same energy. Selectively varying their energies is of great interest for applications because it unlocks the potential to control valley degree of freedom, and offers a new promising way to carry information in next-generation valleytronics. In this proceeding paper, we show that the energy gaps at the two valleys can be shifted relative to each other by means of the optical Stark effect in a controllable valley-selective manner. We discuss the physics of the optical Stark effect, and we describe the mechanism that leads to its valley-selectivity in monolayer TMD tungsten disulfide (WS_2).

Keywords: Optical Stark effect, transition metal dichalcogenide, transient absorption, valleytronics, Floquet, WS_2, monolayer, valley
*gedik@mit.edu

1. INTRODUCTION

Monolayer transition-metal dichalcogenides (TMDs) comprise a new class of atomically thin semiconducting crystals such as MoS_2, WS_2, $MoSe_2$, and WSe_2. They have a honeycomb lattice structure, and a corresponding hexagonal Brillouin zone with two inequivalent valleys, K and K', where the electronic band edges are located. These materials possess a strong spin-orbit coupling inherited from their atomic orbitals. But, unlike their bulk counterparts, the crystalline structure of these monolayer TMDs have no inversion symmetry. This leads to a unique spin-valley coupling at the band edges that results in novel valleytronic properties when interrogated with circularly polarized light [1]. In particular, this system obeys a selection rule where the two valleys couple differently with left and right circularly polarized light. This allows photoexcitation across the band gap that can be made valley-selective. In this way, the electron population imbalance between the two valleys can be utilized to carry information for valleytronic applications.

Alternative approach to control the valley degree of freedom can also be pursued by tuning the energy level between the two valleys. Note that, the two valleys are energetically degenerate because they are protected by time-reversal symmetry. Applying a magnetic field can in principle be used to break time-reversal symmetry and lift the valley degeneracy through Zeeman effect. However, experiments to date have shown an energy splitting by only 1–2 meV at fields commonly accessible in the laboratory [2-4]. In this proceeding paper, we show that the valley degeneracy in monolayer TMD WS_2 can be lifted optically, as we reported recently in E. J. Sie *et. al.*, Nature Materials **14**, 290 (2015) [5]. By applying intense circularly polarized light, which also breaks time-reversal symmetry, the exciton level in each valley can be selectively tuned by as much as 18 meV via the optical Stark effect.

2. THEORY OF THE OPTICAL STARK EFFECT

The physics of the optical Stark effect can be presented semi-classically by a Hamiltonian in which light is represented by classical fields as external perturbation. The perturbed Hamiltonian can be diagonalized to obtain the altered energy levels, and the optical Stark effect can be perceived from the induced change of the energy spectrum. An equilibrium system that is coherently driven by light will acquire newly created photon-dressed states (or Floquet states, [6]) with energy spacing in units of the photon energy. These Floquet states can also be seen from the energy denominator of the energy shift as will be described below. On the other hand, in the quantum-mechanical description of the optical Stark

Ultrafast Bandgap Photonics, edited by Michael K. Rafailov, Eric Mazur, Proc. of SPIE Vol. 9835, 983518 · © 2016 SPIE
CCC code: 0277-786X/16/$18 · doi: 10.1117/12.2223462

Downloaded From: http://proceedings.spiedigitallibrary.org/ on 04/14/2017 Terms of Use: http://spiedigitallibrary.org/ss/termsofuse.aspx

effect, light is represented by quantized oscillators, from which the Floquet states are seen in the quantized photon energy spacing in the energy spectrum. In the following, we will begin by discussing the semi-classical picture of the optical Stark effect, and later compare with the quantum picture.

2.1 Semi-classical physics of the optical Stark effect

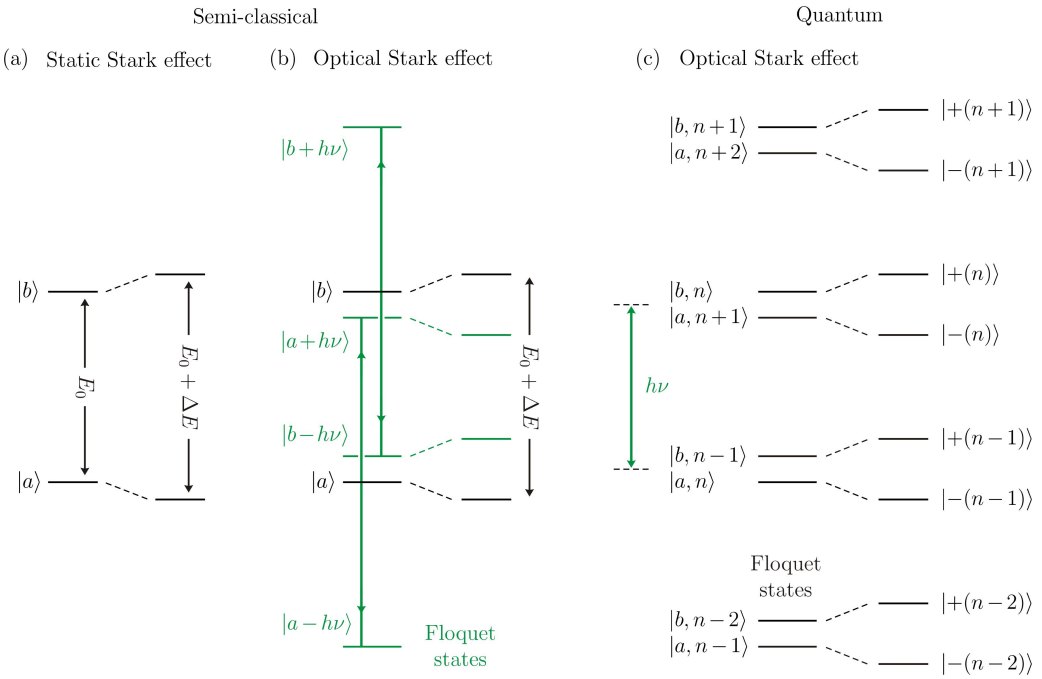

Figure 1. (a) Energy level diagram of the static Stark effect in a two-level system. (b) Semi-classical and (c) quantum description of the optical Stark effect.

The optical Stark effect, in principle, results from induced energy repulsion between two states, similar to the case of the static Stark effect. We consider a two-level atomic system of states $|a\rangle$ and $|b\rangle$ with respective energies of E_a and E_b (Fig 1a), and we put this atom in the presence of static electric field $\mathcal{E}$. Since the atomic orbitals have a definite parity, the Stark effect in atoms starts to emerge from a second-order perturbation with $\mathcal{E}$, inducing a hybridization between states $|a\rangle$ and $|b\rangle$ that results in shifted energy levels by as much as

$$\Delta E_b = \frac{|\langle b|\hat{p}\mathcal{E}|a\rangle|^2}{E_b - E_a} = \frac{\mathcal{M}_{ab}^2|\mathcal{E}|^2}{E_b - E_a} \tag{1}$$

$$\Delta E_a = \frac{|\langle b|\hat{p}\mathcal{E}|a\rangle|^2}{E_a - E_b} = -\frac{\mathcal{M}_{ab}^2|\mathcal{E}|^2}{E_b - E_a} \tag{2}$$

where $\hat{p}$ is the electric dipole moment operator of the atom, $\mathcal{E}$ is the static electric field strength, and $\mathcal{M}_{ab}$ is the polarization matrix element between $|a\rangle$ and $|b\rangle$. Such energy shifts result in a wider separation of the energy levels, also known as the state repulsion, with magnitude

$$\Delta E = 2\frac{\mathcal{M}_{ab}^2|\mathcal{E}|^2}{E_b - E_a} \tag{3}$$

where the magnitude is quadratic in $\mathcal{E}$ and is inversely proportional to the energy separation $E_b - E_a$ before the application of the field (Fig 1a). In the optical Stark effect, the perturbation is written as $\hat{H}'(t) = \hat{p}\mathcal{E}(t)$, where $\mathcal{E}(t) = \mathcal{E}_0 \cos 2\pi\nu t$ is the oscillating electric field with amplitude $\mathcal{E}_0$ and frequency ν. Here, we use a time-dependent perturbation theory [7] to find the shift of the energy levels

$$\Delta E_b(t) = H'_{ab}(t)\exp\left(\frac{i(E_b - E_a)t}{\hbar}\right)\frac{1}{i\hbar}\int_0^t H'_{ab}(t')\exp\left(-\frac{i(E_b - E_a)t'}{\hbar}\right)dt' \tag{4}$$

Downloaded From: http://proceedings.spiedigitallibrary.org/ on 04/14/2017 Terms of Use: http://spiedigitallibrary.org/ss/termsofuse.aspx

where $\Delta E_a(t)$ has a similar expression after switching the indices. We can write the perturbation Hamiltonian as $\hat{H}'(t) = \hat{p}\mathcal{E}_0(e^{i2\pi\nu t} + e^{-i2\pi\nu t})/2$ in order to make apparent the coherent absorption and emission of light from the atomic states. Equation (4) can be evaluated using this perturbation to obtain the time-averaged shift of the energy levels

$$\Delta\bar{E}_b = \frac{1}{2}\left[\frac{\mathcal{M}_{ab}^2\langle\mathcal{E}^2\rangle}{E_b - E_a - h\nu} + \frac{\mathcal{M}_{ab}^2\langle\mathcal{E}^2\rangle}{E_b - E_a + h\nu}\right] \tag{5}$$

$$\Delta\bar{E}_a = -\frac{1}{2}\left[\frac{\mathcal{M}_{ab}^2\langle\mathcal{E}^2\rangle}{E_b - E_a - h\nu} + \frac{\mathcal{M}_{ab}^2\langle\mathcal{E}^2\rangle}{E_b - E_a + h\nu}\right] \tag{6}$$

where $\langle\mathcal{E}^2\rangle = \mathcal{E}_0^2/2$ is the time-averaged value of the electric field squared. These expressions are consistent with the case of the static electric field in equations (1) and (2) in which $h\nu \to 0$ and $\langle\mathcal{E}^2\rangle \to \mathcal{E}_0^2$. In our experiment, $h\nu$ is detuned only slightly below $E_b - E_a$ such that the contribution from the first term to the energy shift dominates, and that of the second term can be neglected. As a result, the energy level separation increases by

$$\Delta\bar{E} = \frac{\mathcal{M}_{ab}^2\langle\mathcal{E}^2\rangle}{E_b - E_a - h\nu} \tag{7}$$

where the energy shift is linearly proportional to the light intensity and is inversely proportional to the light energy detuning from the $E_b - E_a$ transition. This phenomenon is known as the optical Stark effect [8, 9], and it has been routinely employed in the study of atomic physics, and to facilitate the cooling of atoms below the Doppler limit [10].

2.2 Quantum-mechanical description of the optical Stark effect

The optical Stark effect can also be described using the Jaynes-Cummings model [11], where light is represented by quantized oscillators with energy of $h\nu$, with a Hamiltonian

$$\hat{H} = \frac{1}{2}(E_b - E_a)\hat{\sigma}_z + h\nu\hat{a}^+\hat{a} + \frac{1}{2}g(\hat{\sigma}^+\hat{a} + \hat{\sigma}^-\hat{a}^+) \tag{8}$$

where the three terms correspond to the two-level atom, the photon reservoir, and the atom-photon interactions, respectively, g is the atom-photon coupling strength, while the Pauli matrices and the ladder operators are given by

$$\hat{a}|n\rangle = \sqrt{n}|n-1\rangle \tag{9}$$

$$\hat{a}^+|n\rangle = \sqrt{n+1}|n+1\rangle \tag{10}$$

$$\hat{\sigma}_z = |b\rangle\langle b| - |a\rangle\langle a| \tag{11}$$

$$\hat{\sigma}^- = |a\rangle\langle b| \tag{12}$$

$$\hat{\sigma}^+ = |b\rangle\langle a| \tag{13}$$

where $|n\rangle$ is the number of photons. Note that this Hamiltonian only couples states $|a, n+1\rangle$ and $|b, n\rangle$ (see Fig 1c), which we can use as the basis for the Hamiltonian matrix

$$H = h\nu\left(n + \frac{1}{2}\right)\begin{pmatrix}1 & 0\\ 0 & 1\end{pmatrix} + \frac{1}{2}\begin{pmatrix}E_b - E_a - h\nu & \hbar\omega_R\sqrt{n+1}\\ \hbar\omega_R\sqrt{n+1} & -(E_b - E_a - h\nu)\end{pmatrix} \tag{14}$$

which can be diagonalized to give the energies

$$E_{n,\pm} = h\nu\left(n + \frac{1}{2}\right) \pm \frac{1}{2}\sqrt{(E_b - E_a - h\nu)^2 + g^2(n+1)} \tag{15}$$

The optical stark shift of $|a\rangle \to |b\rangle$ optical transition can then be evaluated, after taking a weak field approximation $g \ll E_b - E_a - h\nu$, from which we will obtain an energy shift identical to equation (7).

2.3 Optical Stark effect in semiconductors

Semiconductors have an electronic bandgap that separates the fully-occupied valence band from an unoccupied conduction band. Therefore, the low-energy excitation in semiconductors can often be described as a simplified two-level system, in which the optical Stark effect can also occur. Prior to this work, however, this effect has only been

Downloaded From: http://proceedings.spiedigitallibrary.org/ on 04/14/2017 Terms of Use: http://spiedigitallibrary.org/ss/termsofuse.aspx

reported in a very limited number of materials, with Cu_2O [12], GaAs [13-17] and Ge [18] semiconductors among the few examples. Here we report the observation of the optical Stark effect in a monolayer TMD WS_2, and we found that the effect can be made valley-selective using circularly polarized light [5].

3. METHODS

3.1 Transient absorption spectroscopy

In our experiments, we used a Ti:sapphire amplifier producing laser pulses with duration of 50 fs and at 30 kHz repetition rate. Each pulse was split into two arms. For the pump arm, the pulses were sent to an optical parametric amplifier to generate tunable photon energy below the exciton absorption ($h\nu < E_x$), while for the probe arm the pulses were sent through a delay stage and a white-light continuum generator ($h\nu$ = 1.78–2.48 eV, chirp-corrected). The two beams were focused at the sample, and the probe beam was reflected to a monochromator and a photodiode for lock-in detection [19]. By scanning the grating and the delay stage, we were able to measure $\Delta R/R$ (and hence $\Delta\alpha$) as a function of energy and time delay. Here, $\Delta\alpha(\omega, t) = \alpha(\omega, t) - \alpha_0(\omega)$. The pump and probe polarizations were varied separately by two sets of polarizers and quarter-wave plates, allowing us to perform valley-selective measurements, and an additional half-wave plate for tuning the pump pulse intensity (Fig 2a). The sample consists of high-quality monolayers of WS_2 that were CVD-grown on sapphire substrates [20-22], and all measurements in this study were conducted at ambient condition (300 K, 1 atm).

4. RESULTS

In monolayer WS_2, the energy of the lowest exciton state is 2.00 eV at room temperature (Fig 2b, black). In order to induce an optical Stark effect on this exciton (as simulated and exaggerated for clarity in Fig 2b, dashed), we use pump pulses with photon energy slightly lower than the exciton energy (1.68–1.88 eV). To measure the energy shift we use transient absorption spectroscopy (Fig 2a), which is a powerful technique capable of probing the resulting change in the absorption spectrum $\Delta\alpha$, as simulated in Fig 2c [19]. The unique optical selection rules of monolayer TMDs allow for $\Delta\alpha$ at the K (or K') valley to be measured with valley-specificity by using left (or right) circularly polarized probe light (inset in Fig 2d).

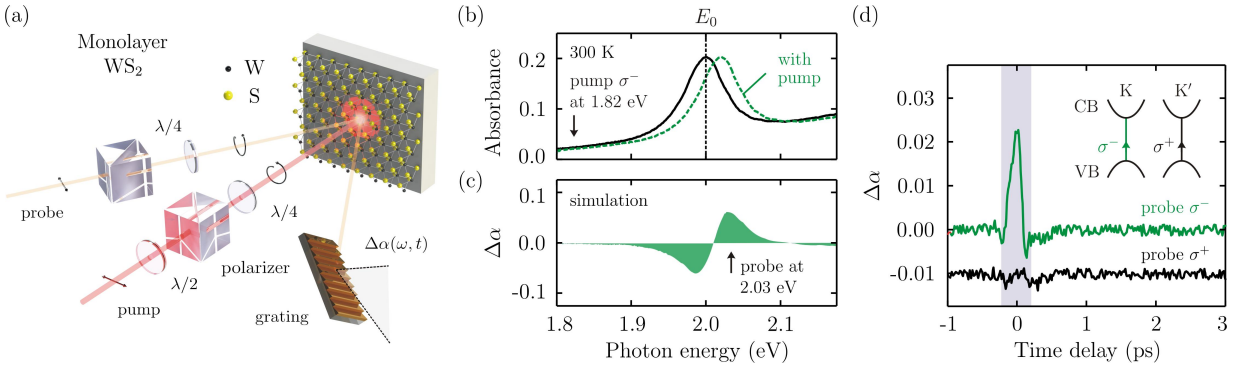

Figure 2. (a) Schematic of transient absorption spectroscopy set-up. (b) Measured absorbance of monolayer WS_2 (black) and hypothetical absorbance curve (dashed) that simulates the optical Stark effect. (c) The simulated change of absorption induced by the pump pulses. (d) Time trace of $\Delta\alpha$, induced by pump pulses of σ^- helicity, measured using probe pulses of the same (σ^-, red) and opposite (σ^+, black, with offset for clarity) helicities.

4.1 Probing the optical Stark effect in monolayer WS_2

In order to search for the optical Stark effect in WS_2, we start by measuring the change in the optical absorption $\Delta\alpha$ as a function of time delay Δt between the pump and probe laser pulses (Fig 2d). We tune the pump photon energy to 1.82 eV so that it is just below the absorption peak, with pulse duration 160 fs at FWHM, fluence 60 μJ/cm^2, and polarization σ^- (left circularly polarized). Since the optical Stark effect is expected to shift the absorption peak to higher energy, the probe photon energy is chosen to be 2.03 eV, which is above the equilibrium absorption peak. Fig 2d shows that when σ^- is used to probe $\Delta\alpha$ (red trace), there is a sharp peak that only exists at $\Delta t = 0$ when the pump pulse is present. This signifies that we are sensitive to a coherent light-matter interaction occurring between the pump pulse and the sample. When σ^+ is used to probe $\Delta\alpha$ (black trace), we observe no discernible signal above the noise level at all time delays.

Downloaded From: http://proceedings.spiedigitallibrary.org/ on 04/14/2017 Terms of Use: http://spiedigitallibrary.org/ss/termsofuse.aspx

This shows that probing the optical Stark effect in this material is strongly sensitive to the selection of pump and probe helicities.

4.2 Time-resolved absorption spectra

Closer examination of $\Delta\alpha$ spectrum in the extended range of 1.85–2.15 eV reveals a faint but noticeable background signal that is present at both valleys. In Fig 3, we present a pair of experimentally measured $\Delta\alpha$ spectra as a function of pump-probe time delay. The probe helicity is tuned to be the same (σ^-, Fig 3a) and opposite (σ^+, Fig 3b) to the pump helicity. Fig 3a shows a distinct feature centered at around $\Delta t = 0$, which consists of positive $\Delta\alpha$ above the original absorption peak and negative below it. In contrast, Fig 3b shows only a faint and premature signal at $\Delta t = 0$. They eventually share a common feature at $\Delta t > 200$ fs, where $\Delta\alpha$ is negative at the absorption peak and positive below it.

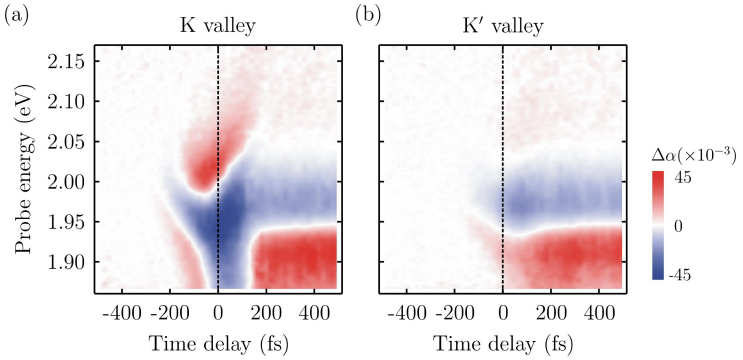

Figure 3. Valley-specific $\Delta\alpha(\omega, t)$ spectra measured using pump-probe pulses of the same (a) and opposite (b) helicities.

The $\Delta\alpha$ spectra at $\Delta t = 0$ shown in Fig 3a indicate that the absorption peak is shifted to higher energy. The non-zero $\Delta\alpha$ values at $\Delta t > 200$ fs in both panels, when the pump pulse no longer persist, are induced by photoexcited excitons, due to excitonic bleaching and biexcitonic absorption [19, 23], and they are present in both valleys. These excitons, however, do not contribute to the optical Stark effect and just add common background signals in both valleys. In the following discussion, we only consider results taken at $\Delta t = 0$ for which the background have been subtracted in order to focus on the optical Stark effect.

4.3 Polarization-resolved absorption spectra

Fig 4a shows the $\Delta\alpha$ spectra at K and K' valleys as induced by σ^- pump pulses. It shows that the optical Stark effect occurs at the K valley, and not at the K' valley. Fig 4b shows identical measurements using instead a σ^+ pump pulses. The effect is now switched to the K' valley. This indicates that the optical Stark effect can be induced valley-selectively using circularly polarized pump pulses, and the effect is well isolated within only the light-driven valley.

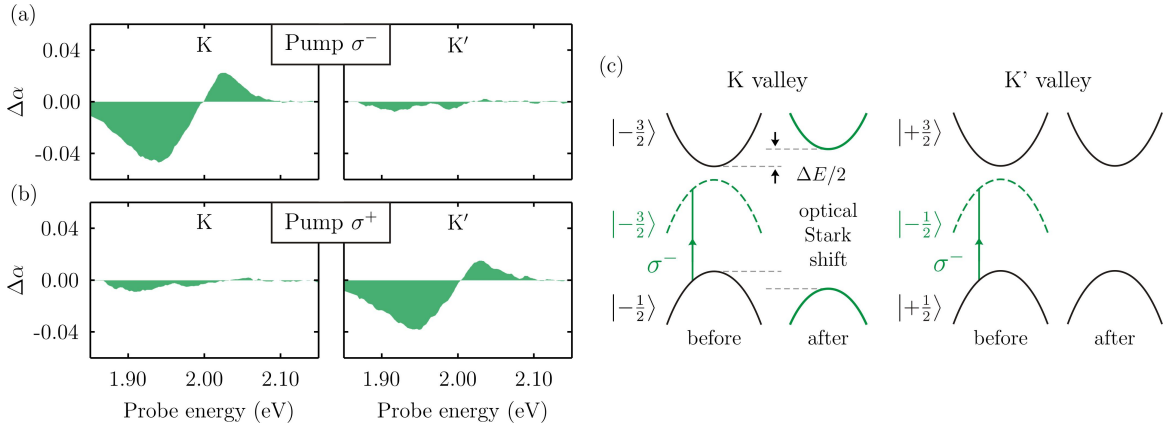

Figure 4. Valley-specific $\Delta\alpha$ spectra induced by (a) σ^- and (b) σ^+ pump pulses probed by using σ^- (K valley) and σ^+ (K' valley) helicities. (c) Band diagrams with the Floquet bands (dashed curves).

Downloaded From: http://proceedings.spiedigitallibrary.org/ on 04/14/2017 Terms of Use: http://spiedigitallibrary.org/ss/termsofuse.aspx

The valley-selectivity of this optical Stark effect arises from the valley selection rules that are present in this class of materials [24-26]. The relevant valence band (VB) and conduction band (CB) in monolayer WS_2 are associated with magnetic quantum numbers m, shown in Fig 4c, which are different between the two valleys. Coherent absorption of light by the VB creates a Floquet band $|\mathrm{VB} + h\nu\rangle$ for which the magnetic quantum numbers are added by the light helicity that carries $\Delta m =$ -1 (σ^-) or +1 (σ^+). Interaction between this Floquet band and the equilibrium CB can lead to a state repulsion provided that they have the same quantum numbers. Note that, the inclusion of excitonic interaction will still preserve the symmetry governing the valley-selectivity and, for the purpose of understanding the effect, the energy of the equilibrium CB is essentially lowered by the exciton binding energy [27]. This explains the valley-selective energy shift we observed in our experiments.

The magnitude of the effect in either valley can also be smoothly tuned as the pump helicity is continuously varied from fully σ^- to fully σ^+, as shown in Fig 5a-b. This arises from the shifting of energy levels as a function of pump polarization, as is schematically depicted in Fig 5c-d. Note that any polarization of the pump pulse can be decomposed into a superposition of σ^- and σ^+ components, for which the effect can be maximized or minimized depending on the valley. This is consistent with the valley selection rules with circularly polarized light in this material.

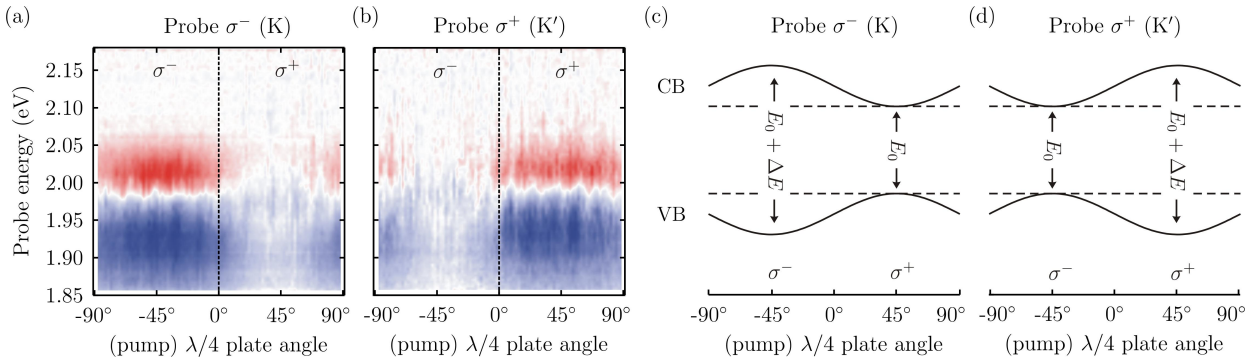

Figure 5. (a, b) Valley-specific $\Delta\alpha(\omega, t = 0)$ spectra measured as a function of pump polarization. (c, d) Band diagrams showing how the energies of the band edges are shifted as a function of pump polarization.

4.4 Determining the energy shift

In order to determine the energy shift, we can compare the obtained $\Delta\alpha$ spectra with what would be obtained from a shifted Gaussian peak. The shifted absorption spectrum can be expressed as

$$\alpha(\omega, \Delta E) = A \exp\left(-\frac{(\omega - \Delta E)^2}{2c^2}\right) \tag{16}$$

where A is the absorption peak, ΔE is the energy shift, c is the FWHM/$2\sqrt{2\ln 2}$, and $\hbar = 1$. The induced absorption spectrum can be derived

$$\Delta\alpha(\omega, \Delta E) = \frac{\omega}{c^2}\alpha(\omega) \tag{17}$$

where we only keep terms in the first order of ΔE. This result has been routinely used to estimate the energy shift ΔE via optical Stark effect through measuring the change in the absorption $\Delta\alpha$ at a particular energy ω [14]. This method, however, is insensitive to distinguishing a peak shift from a peak broadening. Thus, it is crucial to measure the full spectrum of $\Delta\alpha$, performed using transient absorption spectroscopy [19], and verify if the measured $\Delta\alpha$ spectrum profile results from a peak shift. To determine the shift in the peak position, we can integrate the area of this $\Delta\alpha(\omega, \Delta E)$ curve in the range of $0 \leq \omega \leq \infty$, which is referred as the spectral weight transfer (SWT), and by using equations (16) and (17) it can be evaluated as

$$\int_0^\infty \Delta\alpha(\omega, \Delta E)d\omega = A\Delta E \tag{18}$$

By measuring the SWT and the absorption peak A (= 0.2), we can extract the energy shift ΔE due to the optical Stark effect. In our analysis, it is sufficient to integrate $\Delta\alpha$ in the range of $2.00 \leq \omega \leq 2.18$ eV because the signal vanishes beyond this upper limit. We plot the estimated energy shift in Fig 6 (blue circles) as a function of fluence/Δ, together

Downloaded From: http://proceedings.spiedigitallibrary.org/ on 04/14/2017 Terms of Use: http://spiedigitallibrary.org/ss/termsofuse.aspx

with accompanying results measured with smaller (black) and larger (red) laser detuning energies Δ. Not only the results show a linear dependence with fluence but they also share a common slope when plotted this way. This is in excellent agreement with equation (7), which estimates an energy shift of 18 meV measured at the highest fluence. We note that, for a given fluence and energy detuning, this material exhibits the largest optical Stark shift in any materials reported to date.

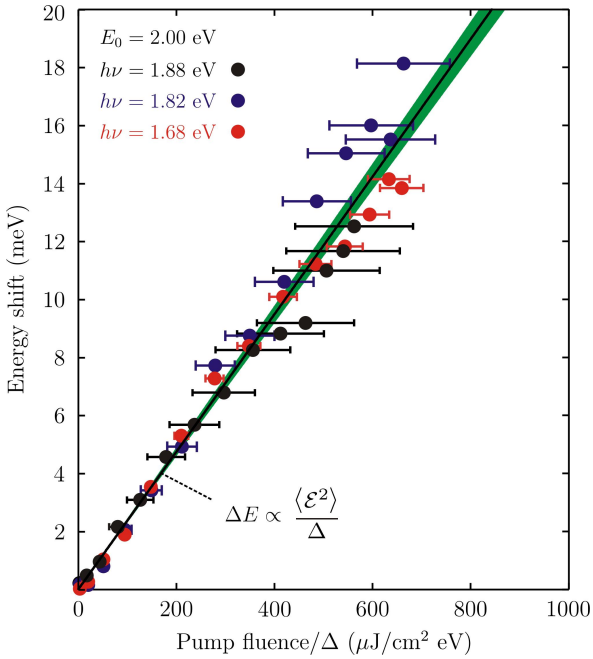

Figure 6. Optical Stark shift as a function of fluence/Δ, showing that all of the data points fall along a common slope. The horizontal error bars correspond to the pump bandwidth of 43 meV. The fitting slope (black line) and the 95% confidence band (green shading) show an excellent agreement with the optical Stark effect.

4.5 Comparison with the predicted Rabi frequency

We can compare the experimentally obtained energy shift with what would be theoretically expected from using an estimated Rabi frequency. In theory, the optical Stark shift is completely described by the transition dipole moment $\mathcal{M}_{ab}$, pump field strength $\mathcal{E}_0$ and pump detuning Δ, which can be calculated and compared with the data in Fig 6. The energy shift has a simple expression given by

$$\Delta E = \frac{(\hbar\omega_R)^2}{2\Delta} \tag{19}$$

where $\hbar\omega_R$ $(= \mathcal{M}_{ab}\mathcal{E}_0)$ is the Rabi frequency. We can estimate for $\mathcal{M}_{ab}$ from the study of quantum well semiconductors [28] given as

$$(\mathcal{M}_{ab})^2 = \left(\frac{eh}{2E_0}\right)^2 \frac{E_g}{m_c} \tag{20}$$

where E_0 (= 2 eV) is the transition energy of the exciton, E_g (= 2.3 eV) is the quasiparticle band gap [29], m_c (= 0.32 m_0) is the effective mass of the conduction electron [30]. This gives $\mathcal{M}_{ab} = 56$ Debye for monolayer WS_2 (1 Debye = 3.3×10^{-30} Cm), which is about twice the value obtained for GaAs quantum wells [31]. For the maximum energy shift of 18 meV, as measured at $\Delta = 180$ meV, we used pump fluence of 120 μJ/cm^2 with pulse width of 160 fs (obtained from Fig 2d). This gives the peak irradiance of I = fluence/width $= \varepsilon_0 c \mathcal{E}_0{}^2/2$ from which we can determine the field strength of $\mathcal{E}_0 = 75$ MV/m and the Rabi frequency of $\hbar\omega_R = 87$ meV. This calculation yields the energy shift of $\Delta E = 21$ meV which is consistent with the measured value of 18 meV in our experiments.

Downloaded From: http://proceedings.spiedigitallibrary.org/ on 04/14/2017 Terms of Use: http://spiedigitallibrary.org/ss/termsofuse.aspx

5. CONCLUSIONS

The observed large valley-selective optical Stark effect in monolayer WS_2 represents a clear demonstration of broken valley degeneracy in a monolayer TMD. Similar results were also obtained in monolayer WSe_2 [32]. This is possible because circularly polarized light breaks time-reversal symmetry, which allows for the lifting of the intervalley spin degeneracy. We have demonstrated so far the optical Stark effect when the pump pulse is red-detuned with respect to the exciton resonance. In principle, this effect can also be demonstrated in the blue-detuned pump regime where we should expect the reverse of the exciton energy shift. However, the situation can become more complicated because of the absorption for photoexcited carriers, which will obscure the signal of the anticipated optical Stark effect. Nevertheless, it will allow us to investigate the effects of real excitons and their many-body interactions on the coherent light-matter interaction in monolayer TMDs, as well as the possibility to create a new topological phase of matter [5, 33-37], and this will be the interest for future works.

ACKNOWLEDGMENTS

The authors acknowledge technical assistance from Qiong Ma and Ya-Qing Bie during the measurement of the equilibrium absorption of monolayer WS_2, and helpful discussions with Zhanybek Alpichshev, Inna Vishik and Yihua Wang. This work is supported by US Department of Energy (DOE) award numbers DE-FG02-08ER46521 and DE-SC0006423 (data acquisition and analysis). Y-H.L. and J.K. acknowledge support from NSF DMR-0845358 (material growth and characterization). Y-H.L. also acknowledges partial support from the Ministry of Science and Technology of the Republic of China (103-2112-M-007-001-MY3). L.F. acknowledges support from the STC Center for Integrated Quantum Materials (CIQM), NSF Grant No. DMR-1231319 (theory).

REFERENCES

[1] Xiao, D., Liu, G.-B., Feng, W., Xu, X. and Yao, W., "Coupled spin and valley physics in monolayers of MoS_2 and other group-VI dichalcogenides," Phys. Rev. Lett. 108, 196802 (2012).
[2] MacNeill, D. et al., "Valley degeneracy breaking by magnetic field in monolayer $MoSe_2$," Phys. Rev. Lett. 114, 037401 (2015).
[3] Aivazian, G. et al., "Magnetic control of valley pseudospin in monolayer WSe_2," Nature Phys. 11, 148 (2015).
[4] Srivastava, A. et al., "Valley Zeeman effect in elementary optical excitations of a monolayer WSe_2," Nature Phys. 11, 141 (2015).
[5] Sie, E. J., McIver, J. W., Lee, Y.-H., Fu, L., Kong, J. and Gedik, N., "Valley-selective optical Stark effect in monolayer WS_2," Nature Mater. 14, 290 (2015).
[6] Shirley, J. H., "Solution of Schrodinger equation with a Hamiltonian periodic in time," Phys. Rev. 138, B979-987 (1965).
[7] Bransden, B. H. and Joachain, C. J., "Physics of Atoms and Molecules. 2nd ed.," Prentice Hall, New Jersey, 2003.
[8] Autler, S. H. and Townes, C. H., "Stark effect in rapidly varying fields," Phys. Rev. 100, 703-722 (1955).
[9] Bakos, J. S., "AC Stark effect and multiphoton processes in atoms," Phys. Rep. 31, 209-235 (1977).
[10] Cohen-Tannoudji, C. N. and Phillips, W. D., "New mechanisms for laser cooling," Phys. Today 43, 33-40 (1990).
[11] Jaynes, E. T. and Cummings, F. W., "Comparison of quantum and semiclassical radiation theories with application to beam maser," Proc. IEEE 51, 89-109 (1963).
[12] Fröhlich, D., Nöthe, A. and Reimann, K., "Observation of the resonant optical Stark effect in a semiconductor," Phys. Rev. Lett. 55, 1335-1337 (1985).
[13] Mysyrowicz, A. et al., "Dressed excitons in a multiple-quantum-well structure: Evidence for an optical Stark effect with femtosecond response time," Phys. Rev. Lett. 56, 2748-2751 (1986).
[14] Joffre, M., Hulin, D., Migus, A. and Antonetti, A., "Dynamics of the optical Stark effect in semiconductors," J. Mod. Opt. 35, 1951-1964 (1988).
[15] Chemla, D. S. et al., "The excitonic optical Stark effect in semiconductor quantum wells probed with femtosecond optical pulses," J. Lumin. 44, 233-246 (1989).
[16] Sieh, C. et al., "Coulomb memory signatures in the excitonic optical Stark effect," Phys. Rev. Lett. 82, 3112-3115 (1999).

Downloaded From: http://proceedings.spiedigitallibrary.org/ on 04/14/2017 Terms of Use: http://spiedigitallibrary.org/ss/termsofuse.aspx

[17] Hayat, A. et al., "Dynamic Stark effect in strongly coupled microcavity exciton polaritons," Phys. Rev. Lett. 109, 033605 (2012).
[18] Koster, N. S. et al., "Giant dynamical Stark shift in germanium quantum wells," Appl. Phys. Lett. 98, 161103 (2011).
[19] Sie, E. J., Frenzel, A. J., Lee, Y.-H., Kong, J. and Gedik, N., "Intervalley biexcitons and many-body interactions in monolayer MoS_2," Phys. Rev. B 92, 135417 (2015).
[20] Lee, Y.-H. et al., "Synthesis of large-area MoS2 atomic layers with chemical vapor deposition," Adv. Mat. 24, 2320-2325 (2012).
[21] Lee, Y.-H. et al., "Synthesis and transfer of single-layer transition metal disulfides on diverse surfaces," Nano Lett. 13, 1852-1857 (2013).
[22] Gutiérrez, H. R. et al., "Extraordinary room-temperature photoluminescence in triangular WS_2 monolayers," Nano Lett. 13, 3447-3454 (2012).
[23] Mai, C. et al., "Many-body effects in valleytronics: Direct measurement of valley lifetimes in single-layer MoS_2," Nano Lett. 14, 202-206 (2014).
[24] Mak, K. F., He, K., Shan, J. and Heinz, T. F., "Control of valley polarization in monolayer MoS_2 by optical helicity," Nature Nano. 7, 494-498 (2012).
[25] Zeng, H., Dai, J., Yao, W., Xiao, D. and Cui, X., "Valley polarization in MoS_2 monolayers by optical pumping," Nature Nano. 7, 490-493 (2012).
[26] Cao, T. et al., "Valley-selective circular dichroism of monolayer molybdenum disulphide," Nature Comms. 3, 887 (2012).
[27] Combescot, M., "Optical Stark effect of the exciton. II. Polarization effects and exciton splitting," Phys. Rev. B 41, 3517-3533 (1990).
[28] Asada, M., Kameyama, A. and Suematsu, Y., "Gain and intervalence band absorption in quantum-well lasers," IEEE J. Quantum Electron. 20, 745-753 (1984).
[29] Chernikov, A. et al., "Exciton binding energy and nonhydrogenic Rydberg series in monolayer WS_2," Phys. Rev. Lett. 113, 076802 (2014).
[30] Berkelbach, T. C., Hybertsen, M. S. and Reichman, D. R., "Theory of neutral and charged excitons in monolayer transition metal dichalcogenides," Phys. Rev. B 88, 045318 (2013).
[31] Schmitt-Rink, S. and Chemla, D. S., "Collective excitations and the dynamical Stark effect in a coherently driven exciton system," Phys. Rev. Lett. 57, 2752-2755 (1986).
[32] Kim, J. et al., "Ultrafast generation of pseudo-magnetic field for valley exciton in WSe_2 monolayers," Science 346, 1205 (2014).
[33] Inoue, J. and Tanaka, A., "Photoinduced transition between conventional and topological insulators in two-dimensional electronic systems," Phys. Rev. Lett. 105, 017401 (2010).
[34] Kitagawa, T., Oka, T., Brataas, A., Fu, L. and Demler, E., "Transport properties of nonequilibrium systems under the application of light: Photoinduced quantum Hall insulators without Landau levels," Phys. Rev. B 84, 235108 (2011).
[35] Lindner, N. H., Refael, G. and Galitski, V., "Floquet topological insulator in semiconductor quantum wells," Nature Phys. 7, 490-495 (2011).
[36] Bernevig, B. A., Hughes, T. L. and Zhang, S. C., "Quantum spin Hall effect and topological phase transition in HgTe quantum wells," Science 314, 1757-1761 (2006).
[37] Perez-Piskunow, P. M., Usaj, G., Balseiro, C. A. and Torres, L. E. F. F., "Floquet chiral edge states in graphene," Phys. Rev. B 89, 121401(R) (2014).

Downloaded From: http://proceedings.spiedigitallibrary.org/ on 04/14/2017 Terms of Use: http://spiedigitallibrary.org/ss/termsofuse.aspx